JOURNAL OF GEOPHYSICAL RESEARCH, VOL. 104, NO. D3, PAGES 3527-3542, FEBRUARY 20, 1999

Isolating nitrated and aromatic aerosols and nitrated aromatic gases as sources of ultraviolet light absorption

Mark Z. Jacobson

Department of Civil and Environmental Engineering, Stanford University, Stanford, California

Abstract. Measurements in 1973 and 1987 showed that downward ultraviolet (UV) irradiances within the boundary layer in Los Angeles were up to 50% less than those above the boundary layer. Downward total solar irradiances were reduced by less than 14% in both studies. It is estimated that standard gas and particulate absorbers and scatterers accounted for only about 52-62% of the observed UV reductions at Claremont and Riverside. It is hypothesized that absorption by nitrated and aromatic aerosol components and nitrated aromatic gases caused at least 25-30% of the reductions (with aerosols accounting for about 4/5 of this percent). The remaining reductions are still unaccounted for. Absorbing aerosol components include nitrated aromatics, benzaldehydes, benzoic acids, aromatic polycarboxylic acids, phenols, polycyclic aromatic hydrocarbons, and nitrated inorganics. Many of these species have been observed to date in atmospheric particles, and absorption coefficient data indicate many are strong absorbers at long UV wavelengths. Since aerosols containing nitrated or aromatic aerosols have been observed widely in many areas aside from Los Angeles the finding may account for a portion of UV extinction in those regions as well. In Los Angeles, the finding may be important for predicting smog evolution, since UV reductions associated with high aerosol loadings were estimated to cause a 5-8% decrease in ozone mixing ratios in August 1987. Further laboratory and field studies are needed to quantify better the extent of UV absorption due to nitrated and aromatic aerosols and nitrated aromatic gases.

1. Introduction

Near-ultraviolet (UV) irradiance (0.25-0.38 μm) comprises only 5% of total solar irradiance but is important because it affects biological systems and drives atmospheric photochemistry. High dosages of UVB radiation (0.29-0.32 μm) damage floating marine organisms, vegetation, and human skin tissue. Many inorganic and organic gases also dissociate following UV absorption. The products of these reactions are responsible for smog production in urban air and ozone production in the free troposphere.

This study was motivated by two sets of UV measurements in the Los Angeles basin. *Peterson et al.* [1978] found that downward direct plus diffuse (global) surface UV irradiances (0.295-0.385 μm), measured with Eppley UV photocell radiometers in autumn 1973, differed between locations in the basin and at Mount Disappointment, above the basin, by up to 50%. Similar measurements from the Southern California Air Quality Study (SCAQS) period of August 26-29, 1987, indicated that peak downward global surface UV irradiances (0.295-0.385 μm) at central Los Angeles (elevation 87 m), Claremont (364 m), and Riverside (249 m) were about 22%, 33%, and 48% less, respectively, than those at Mount Wilson (1739 m). In both studies, downward global solar irradiances (0.285-2.8 μm), measured with Eppley precision spectral pyranometers, differed between boundary-layer sites and above-boundary-layer sites by 8-14%.

The uncertainty of the downward UV and total solar measurements is not exactly known but may be within ±5%. *Zeng et al.* [1994] estimated errors of ±5% from a UV spectral irradiance instrument. *Kato et al.* [1997] found that downward solar irradiances at the surface measured by three independently calibrated unshaded pyranometers varied over a range of 5%. These possible errors should not significantly affect the conclusions of this paper, since the paper focuses more on the relative differences of irradiance measured with the same instrument at different locations rather than absolute values of the measurements.

Although *Peterson et al.* [1978] believed aerosols within air pollution caused much of the UV reductions in Los Angeles, they did not isolate the constituents of aerosols responsible for the reductions. Large reductions in UV irradiance in the presence of pollutants have also been observed in Athens, Greece [*Varotsos et al.*, 1995; *Repapis et al.*, 1998], western North Carolina [*Wenny et al.*, 1998], and in the Alps [*Reiter et al.*, 1982; *Blumthaler et al.*, 1994]. In these studies, aerosols were also thought to attenuate some of the UV irradiance, but the constituents of aerosols responsible for the reductions were not isolated.

The downward global UV irradiance at the ground is affected by incident radiation at the top of the atmosphere, gas, aerosol, and cloud drop scattering and absorption of incident radiation, and downward scattering of ground-reflected radiation. The goal of this study was to isolate the extinction process(es) responsible for reductions in downward global UV irradiance in Los Angeles. *Ambach and Blumthaler* [1994] found that, in an environment less polluted than Los Angeles (a mountain station at Jungfraujoch, Switzerland, versus a valley station at Innsbruck, Austria), reductions in UVB, UVA, and total solar irradiance with decreasing altitude were 17.7%, 9.3%, and 8% per km, respectively. Since UVB ≈ 1/3 UVA irradiance, the total UVA+UVB irradiance reduction in this case was about 11.4%. It can be compared with a 13% per

Paper number 1998JD100054.
0148-0227/99/1998JD100054$09.00

km UVA+UVB irradiance reduction at central Los Angeles, a 24% per km reduction at Claremont, and a 31% reduction per km at Riverside during SCAQS. The incremental UV reductions at Claremont and Riverside in comparison with those at central Los Angeles and Innsbruck suggest that excess pollutants, not background ozone, Rayleigh scattering, or background particles, were present at Claremont and Riverside. Indeed, analytical and model calculations indicate that background gas and aerosol scattering and gas absorption were responsible for only a portion of the UV reductions at Claremont and Riverside. Standard aerosol materials known to absorb UV wavelengths include elemental carbon and soil components [e.g., *Krekov*, 1993; *Gillette et al.*, 1993; *Sokolik et al.*, 1993]. When these absorbers, together with standard scatters, were included in their observed concentrations in analytical and model calculations, only 52-62% of the observed reductions at Claremont and Riverside could be accounted for.

The purpose of this study is to show that previously unconsidered absorption by certain aerosol and gas components is a plausible cause of a portion of the remaining reduction in downward global UV irradiance observed in Los Angeles. To date, several studies of UV irradiance have been carried out [*Reiter et al.*, 1982; *Madronich*, 1987; *Liu et al.*, 1991; *Blumthaler et al.*, 1992; *van Weele and Duynkerke*, 1993; *Zeng et al.*, 1994; *Wang and Lenoble*, 1994; *Ruggaber et al.*, 1994; *Blumthaler et al.*, 1994; *Forster*, 1995; *Lu and Khalil*, 1996; *Varotsos et al.*, 1995; *Wendisch et al.*, 1996; *Dickerson et al.*, 1997; *Repapis et al.*, 1998; *Wenny et al.*, 1998]. This is the first study to consider the effects of absorption by nitrated and aromatic aerosol components and nitrated aromatic gases on UV-irradiance reduction.

Because nitrated and aromatic aerosols and nitrated aromatic gases have been observed widely, their ability to absorb UV radiation may affect UV irradiance beyond urban regions. Over the continental United States, organic material typically accounts for 5-50% of total fine particle mass and is often the largest component in particles after sulfate and nitrate [*Saxena and Hildemann*, 1996]. Simulations by *Liousse et al.* [1996] indicate that annual average near-surface particulate organic carbon concentrations over all continents, except Antarctica, and nearby coastal regions range from 0.2 to 14 $\mu g\ m^{-3}$, with continental areas typically affected by concentrations greater than 2 $\mu g\ m^{-3}$. *Novakov et al.* [1997a] measured particulate carbon up to 3 km altitude onshore and offshore of the eastern coast of the United States and found concentrations up to 9.9 $\mu g\ m^{-3}$. Organic carbon made up about 90% of the total carbon.

Nitrates within particles have been observed extensively throughout the lower troposphere [e.g., *Chow et al.*, 1994; *Saxena and Hildemann*, 1996; *Li et al.*, 1997]. Nitrated phenols, in particular have been observed in aerosols and raindrops in clean and polluted locations in Japan, Los Angeles, Portland, Germany, and Switzerland [*Nojima et al.*, 1983; *Pankow et al.*, 1983; *Rippen et al.*, 1987; *Leuenberger et al.*, 1988]. *Nojima et al.* [1983] found that 4-nitrophenol and 2-methyl-4-nitrophenol (nitrocresol), which originate from gas-phase photochemical reactions of benzene and toluene, respectively, with nitrogen dioxide, were the main nitrophenols found in suspended particulates in Yokohama, Japan. *O'Brien et al.* [1975] found that organic material at Los Angeles and Riverside consisted of 17 (+/-4)% organic nitrates, 22 (+/-14)% monocarboxylic acids, and 10 (+/-6)% dicarboxylic acids. They also found that about one acid molecule in nine contains an organic nitrate group. *Mylonas et al.* [1991] found that organonitrates represented about 12% of total carbon in Los Angeles aerosols.

The hypothesis that nitrated and aromatic aerosols and nitrated aromatic gases were responsible for part of the downward global UV irradiance reductions at Claremont and Riverside is supported by four factors. First, radiative transfer theory in conjunction with observed and calculated extinction coefficients indicate that UV irradiance reductions were affected by absorption. Second, commonly considered absorbers cannot fully account for the observed UV reductions. Third, preferential UV absorption characteristics of nitrated and aromatic aerosols and nitrated aromatic gases may partly explain why observed UV reductions far exceeded observed total solar reductions in Los Angeles. Fourth, model predictions of downward global UV irradiance improved when optical properties of nitrated and aromatic organics and nitrated aromatic inorganics were accounted for. Each factor is discussed below.

2. Role of Aerosol Absorption in UV Irradiance Reductions

Reductions in downward UV irradiance in Los Angeles are hypothesized to be due, in large part, to absorption. Table 1, which shows calculated reductions in downward global irradiance for given single-scattering albedos (ω_0), optical depths (τ), and asymmetry parameters (g_0), supports this hypothesis. The single-scattering albedo is the ratio of scattering extinction to total extinction. Interpolations from Table 1 indicate that, when $g_0 = 0.5$, downward global irradiance reductions of 48%, such as observed at Riverside, occur only when $\omega_0 \ll 0.5$ and $\tau = 0.5$, $\omega_0 \approx 0.6$ and $\tau = 1.0$, or $\omega_0 \approx 0.91$ and $\tau = 2.0$. In all cases, significant absorption is required to reduce downward irradiance.

Figure 9 of *Jacobson* [1997a] shows predicted versus observed scattering and absorption extinction coefficients at Claremont, California, on August 27, 1987, at 1630 PST. At λ=0.5 μm wavelength, the predicted scattering coefficient, absorption coefficient, and single-scattering albedo were about σ_s=0.21, σ_a=0.022 km^{-1}, and ω_0=0.9, respectively. These values nearly matched observations. For ω_0=0.9 and g_0 = 0.5, Table 1 indicate that τ=0.34 is necessary to obtain a 10% downward visible irradiance reduction at Claremont, which is near what *Peterson et al.* [1978] found for total solar reductions in the basin. This τ would be equivalent to a

Table 1. Percent Reduction in Calculated Downward Direct Plus Diffuse UV Irradiance Through the Given Optical Depth (τ) for the Given Asymmetry Parameter (g_0) and Single-Scattering Albedo (ω_0) When the Zenith Angle is 25° and the Surface Albedo is 8%

	$g_0 = 0.5$			$g_0 = 0.75$		
ω_0	$\tau = 0.5$	$\tau = 1.0$	$\tau = 2.0$	$\tau = 0.5$	$\tau = 1.0$	$\tau = 2.0$
0.5	-29.4	-51.7	-78.0	-26.6	-47.2	-73.3
0.8	-18.6	-35.7	-61.1	-13.8	-27.7	-50.3
0.95	-11.8	-23.4	-42.8	-5.7	-13.8	-28.2
1.0	-9.2	-18.3	-33.0	-2.5	-8.2	-17.3

Results were obtained from a four-stream radiative calculation.

boundary-layer thickness of 1.5 km applied to the observed total extinction coefficient of 0.23 km^{-1} at λ=0.5 μm.

Figure 9 of *Jacobson* [1997a] shows that the predicted scattering and absorption extinction coefficients at λ=0.3 μm at Claremont were about σ_s=0.245 and σ_a=0.032 km^{-1}, respectively, giving ω_0=0.88 at this wavelength. These calculations did not include the effects of UV absorption by nitrated or organic aerosol components. Applying a 1.5 km boundary layer thickness to $\sigma_s+\sigma_a$ gives τ=0.44 at λ=0.3 μm. When τ=0.44 and ω_0=0.88, the downward irradiance reduction from Table 1 is 13%. Since this reduction is much less than the observed 33% UV reduction at Claremont, additional UV absorption or scattering must have been occurring at Claremont.

Suppose UV scattering coefficients were actually 3 times larger (0.74 km^{-1}) than estimated above. This might occur, for instance, if accumulation-mode particles were pure scatterers (nonabsorbers) and their single particle scattering efficiencies at UV wavelengths were 3 times those at visible wavelengths. In reality, the presence of elemental carbon together with pure scatterers dampens effective single-particle scattering efficiencies. Nevertheless, in the threefold scattering case, ω_0=0.96 (since σ_a=0.032 km^{-1}), and the optical depth through a 1.5 km layer is τ=1.15. Under such conditions, Table 1 indicates an irradiance reduction of near 25%, which is still short of the 33% reduction required for Claremont. At Riverside the shortfall is even greater. The most likely mechanism to account for remaining UV reduction is absorption. This theory is supported by Table 1, which indicates that, for any given optical depth, lower values of ω_0 reduce downward irradiance more than higher values of ω_0. Thus for a given quantity of pollutants, absorption is more effective than scattering at reducing downward UV irradiance.

3. Observed Aerosol Concentrations During SCAQS

A clue to a plausible source of additional absorption in the basin was the fact that downward UV irradiances decreased from central Los Angeles to Claremont to Riverside. Each of these locations is successively farther inland. Generally, locations farther inland in the basin have higher aerosol concentrations and a greater percentage of aerosol material formed from gas-to-particle conversion than do locations near the coast. Both features are illustrated by Table 2. The table shows that, during the SCAQS period, the near-surface total sub-10-μm dry-aerosol concentration at 1230 PST on August 27 increased from 74.5 to 175.6 $\mu g\ m^{-3}$ between central Los Angeles and Riverside. The table also shows that aerosol nitrate, which forms from gas-to-particle conversion, increased in concentration from 9.9 at Los Angeles to 25.4 at Claremont to 63.8 $\mu g\ m^{-3}$ at Riverside. Of the species shown in the table, nitrate was the most abundant aerosol component inland (except possibly liquid water).

Table 2. Observed Near-Surface Concentrations ($\mu g\ m^{-3}$) of Several Components Within Particles < 10 μm in Diameter at Three Sites at 1230 PST on August 27, 1987

Particle Component	Central Los Angeles	Claremont	Riverside
Elemental carbon	5.2	4.9	4.2
Organic carbon	10.8	18.6	16.6
Nitrate	9.9	25.4	63.8
Sulfate	8.0	8.2	9.8
Chloride	0.16	0.0	0.07
Ammonium	8.0	9.5	25.1
Sodium	2.4	1.2	1.2
Total mass	74.5	89.2	175.6

Elemental carbon, an emitted aerosol component, decreased in concentration from central Los Angeles to Riverside, suggesting that it was unlikely to be the cause of the excess UV reductions at Claremont and Riverside. Sulfate, sodium, and chloride concentrations did not change significantly from central Los Angeles to Riverside or were low. Ammonium concentrations increased from west to east, since ammonia gas emissions are greatest in the eastern basin and ammonium forms from gas-to-particle conversion of ammonia gas.

Table 2 shows that aerosol organic carbon, which is emitted and forms from gas-to-particle conversion, increased in concentration from central Los Angeles to Claremont but decreased slightly in concentration from Claremont to Riverside. It is hypothesized that nitrated aromatic aerosols and nitrated aromatic gases caused some of the excess UV reduction at Claremont compared with central Los Angeles. Additional nitration of aromatic aerosols and gases may have caused some of the excess UV reduction at Riverside compared with Claremont. It should be noted that the observations in Table 2 were obtained near the surface. *Wakimoto and McElroy* [1986] found that strong elevated aerosol layers are prevalent above Riverside and other cities near the San Bernardino Mountains. Aerosol layers above Claremont, near the San Gabriel Mountains, are weaker. Thus data from the table, alone, cannot be used to support the hypotheses made here.

4. Absorption Characteristics of Nitrated/Aromatic Aerosols/Gases

The extent of absorption by a substance at a given wavelength is determined in a model with imaginary and real refractive index data. Such data are required as inputs into Mie scattering and absorption calculations. Whereas measured UV imaginary index of refraction data for organic particulate substances are sparse; measured absorption coefficient data are fairly abundant. Such data are converted here to imaginary refractive index data.

In one measurement study, the UV imaginary refractive index of liquid nitrobenzene was found to increase from 0.1 at 0.4 μm to 0.395 at 0.28 μm [*Foster*, 1992], as seen in Figure 1. The figure shows that, although its longest peak wavelength of absorption (0.28 μm) is shorter than most UV wavelengths reaching the ground, nitrobenzene absorbs significantly between 0.3 and 0.4 μm.

4.1. Imaginary Refractive Index Calculations

Here, imaginary refractive indices of several aerosol components are estimated from molar absorption spectra data. *Hirayama* [1967], *Perkampus* [1992], and *Lide and Milne* [1995] give molar absorption coefficient data for numerous organic compounds. The fist and third sources provide absorption coefficients at peak UV wavelengths; whereas the second source provides continuous absorption coefficient curves for the UV spectrum. A molar absorption coefficient (ε, $M^{-1}\ cm^{-1}$, base 10) of a substance quantifies the attenuation of

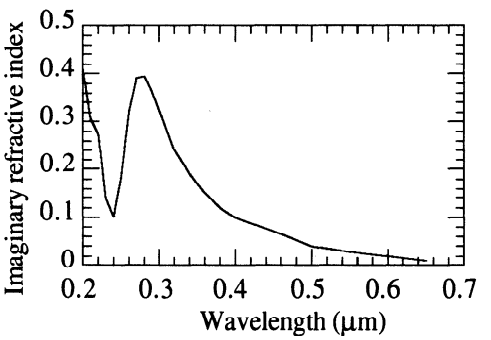

Figure 1. Imaginary index of refraction of liquid nitrobenzene versus wavelength. Data from *Foster* [1992].

incident radiance (I_0, W m^{-2} μm^{-1} sr^{-1}) as it passes through a distance x (cm) of a fluid containing the substance. The attenuated irradiance is

$$I = I_0 10^{-\varepsilon M x} \tag{1}$$

where M is the molality (M, moles per liter of solution) of the substance. The fluid may be a gas or liquid. Absorption coefficients of a substance differ not only between the gas and liquid phases, but also among different solvents in the liquid phase. Typical solvents used for determining liquid-phase absorption coefficients are methyl alcohol, ethyl alcohol, water, hexane, and heptane.

For a pure liquid (where the liquid is both solute and solvent) of density ρ (grams per cubic centimeter of liquid) and molecular weight m (grams per mole), the liquid's molarity is $M = 1000\rho/m$, and (1) becomes

$$I = I_0 10^{-\varepsilon 1000 \rho x/m} \tag{2}$$

The imaginary index of refraction (κ, unitless) at wavelength λ of a pure liquid is related to incident radiance, final radiance, and distance by

$$I = I_0 \exp(-4\pi\kappa x/\lambda) \tag{3}$$

Equating (2) with (3) gives the imaginary index of refraction of a pure liquid at a given wavelength as a function of the molar absorption coefficient (base 10) as

$$\kappa = 1000 \ln(10) \frac{\varepsilon \rho \lambda}{4\pi m} \tag{4}$$

Attenuation of incident radiance through a gas or liquid can also be written in terms of a molecular absorption cross section (b, cm^2 molecule^{-1}, base e) with

$$I = I_0 \exp(-bNx) \tag{5}$$

where N is the number concentration (molecules per cubic centimeter of fluid) of the gas or liquid. Combining $N = MA/1000$, where A is Avogadro's number (molecules per mole) with (1) and (5) gives the molecular absorption cross section (base e) in terms of the molar absorption coefficient (base 10) as

$$b = 1000 \ln(10) \frac{\varepsilon}{A} \tag{6}$$

Using b for the liquid phase and combining (4) with (6) gives another equation for the imaginary refractive index [*Jackson*, 1975; *Beyer et al.*, 1996],

$$\kappa = \frac{bA\rho\lambda}{4\pi m} \tag{7}$$

Table 3 lists liquid-phase absorption and scattering characteristics of several organic substances, including nitrated aromatics, benzaldehydes, other aldehydes, benzoic acids, aromatic polycarboxylic acids, phenols, polycyclic aromatic hydrocarbons (PAHs), and certain organic bases. The table includes, among other parameters, longest peak UV absorption wavelengths, corresponding liquid-phase molar absorption coefficients (and the solvents in which they were measured), calculated imaginary refractive indices from (4) at the peak wavelength, and calculated liquid-phase molecular absorption cross sections from (6). The table also indicates whether each substance has been observed to date in ambient or emitted aerosols. The table indicates that nitrated aromatics, PAHs, and benzaldehydes are the most efficient UVA and UVB organic absorbers in terms of their imaginary refractive indices and absorption wavelengths. Most monocarboxylic and dicarboxylic acids, not shown in the table, have their longest peak absorption wavelengths shorter than 0.27 μm. Their absorption tails may reach 0.3-0.4 μm in some cases.

Although Table 3 gives only peak UV absorption characteristics, the absorptivities of many nitrated aromatics are strong throughout the UV spectrum. This is seen in Figure 2, which shows imaginary refractive index estimates versus wavelength for five liquid-phase nitrated and/or aromatic chemicals. The figure was derived by applying (6) to molar absorption coefficient data from *Perkampus* [1992]. As shown in Table 3, most of the species in Figure 2 have been observed in the atmosphere.

4.2. Effect of Functional Groups on Absorptivity

The strong near-UV absorptivity of nitrated aromatics occurs because the substitution of a nitrate group onto a benzene ring shifts the peak wavelength of absorption by 0.057 μm toward longer wavelengths [e.g., *Dean*, 1992]. The relatively strong near-UV absorptivity of benzaldehydes and benzoic acids results because the addition of an aldehyde or acid group to a benzene ring shifts the peak wavelength by 0.046 μm and 0.0255 μm, respectively [Dean, 1992]. The addition of a nitrate group to a nonaromatic organic shifts the peak wavelength of absorption to a longer wavelength as well. Thus the addition of a nitrate group to carboxylic or dicarboxylic acids, as found by *O'Brien et al.* [1975], would increase the UV absorption capabilities of these acids.

4.3. Effect of pH on Absorptivity

Not only does the addition of certain functional groups change the peak wavelength of absorption, but so does dissociation in solution. *Alif et al.* [1987, 1990, 1991] found that the anionic forms of aqueous 4-nitrophenol, 3-nitrophenol, and 2-nitrophenol absorbed more strongly and at longer wavelengths than the molecular forms of these chemicals. For instance, the anionic form of 4-nitrophenol absorbed at 0.398 μm with ε = 18,500 M^{-1} cm^{-1} (κ = 1.43), whereas the molecular form absorbed at 0.317 μm with ε = 10,300 M^{-1} cm^{-1} (κ = 0.64). 4-nitrophenol has a pKa of 6.98. Figure 2 shows the relative imaginary refractive indices,

Table 3. Several Observed or Possible Organic Aerosol Components With Longest Peak UV Absorption Wavelength (λ_p) Greater Than 0.25 μm

Chemical Name	λ_p nm	S	Ref. A	Ref. B	m g mol^{-1}	ρ g cm^{-3}	ε M^{-1} cm^{-1} (Solvent)	κ	b_{liq} cm^2 molecule^{-1}	b_{gas} cm^2 molecule^{-1}	n
Nitrated aromatics											
2,4-Dimethyl-6-nitrophenol	[a]446	?			167.16	z2	[a]3981(N)	0.25	1.52(-17)		?
3,4-Dimethyl-6-nitrophenol	[a]432	?			167.16	z2	[a]5011(N)	0.31	1.92(-17)		?
2,3-Dimethyl-6-nitrophenol	[a]430	?			167.16	z2	[a]5012(N)	0.31	1.92(-17)		?
3,6-Dimethyl-2-nitrophenol	[a]424	?			167.16	z2	[a]794(N)	0.048	3.04(-18)		?
3,4-Dimethyl-2-nitrophenol	[a]419	?			167.16	z2	[a]794(N)	0.047	3.04(-18)		?
3,5-Dimethyl-2-nitrophenol	[a]412	?			167.16	z2	[a]1585(N)	0.093	6.06(-18)		?
3,6-Dimethyl-4-nitrophenol	[a]410	?			167.16	z2	[a]19,953(N)	1.16	7.63(-17)		?
4-Nitrophenol anion	[l]400	?			138.10	z6	[l]18,000(N)	1.41	6.88(-17)		?
4-Nitrobenzenamine (*p*-Nitroaniline)	[l]373	1			138.13	1.424	[l]15,400(E)	1.09	5.89(-17)		?
3-Nitrobenzenamine (*m*-Nitroaniline)	371	2			138.13	0.991	1090(M)	0.055	4.17(-18)		?
1,4-Dimethoxy-2-nitrobenzene	357	1			183.16	1.1666	2455(M)	0.10	9.39(-18)		?
2-Nitrophenol	[l]351	2	d,e,h,i		139.11	1.2942	[l]3050(W)	0.18	1.17(-17)		1.5723
3,5-Dimethyl-4-nitrophenol	[a]351	?			167.16	z2	[a]1585(A)	0.078	6.06(-18)		?
2,4,6-Trinitrophenol	350	2			229.11	z1	6740(M)	0.32	2.58(-17)		1.763
2,6-Dinitrophenol	[l]350	1	d		184.11	z1	[l]5200(C)	0.30	1.99(-17)		?
3,6-Dimethyl-2-nitrophenol	347	?			167.16	z2	1202(E)	0.06	4.60(-18)		?
4-Nitro-1,3-benzenediol	337	?			155.11	z3	10,715(Cx)	0.54	4.10(-17)		?
3-Methyl-2,4,6-trinitrophenol	335	2			243.13	z1	3467(N)	0.15	1.33(-17)		?
1,3,5-Trimethyl-2-nitrobenzene	334	?			165.19	1.51	552(M)	0.031	2.11(-18)		?
3-Nitrophenol	[l]333	2			139.11	1.2797	[l]1950(W)	0.11	7.46(-18)		?
2,3-Dinitrophenol	329	2			184.11	1.681	2670(M)	0.15	1.02(-17)		?
5-Nitroisoquinoline	329	2			174.16	z4	4490(M)	0.22	1.72(-17)		?
1,2-Dimethoxy-4-nitrobenzene	323	1	m		183.16	1.1888	7943(E)	0.31	3.04(-17)		?
2,6-Dimethyl-4-nitrophenol	[a]323	?			167.16	z2	[a]10,000(A)	0.46	3.82(-17)		?
2,4-Dimethoxy-1-nitrobenzene	321	1			183.16	1.1876	6026(E)	0.23	2.30(-17)		?
1-Methoxy-2-nitrobenzene	321	1			153.14	1.254	?(M)	?	?		1.5161
2-Methyl-4-nitrophenol (nitrocresol)	319	2	d, f		153.14	1.5744	9010(M)	0.54	3.44(-17)		?
4-Nitrophenol	[l]317	2	d, h		139.11	1.479	[l]9500(W)	0.59	3.63(-17)		?
1-Methoxy-3-nitrobenzene	306	1			153.14	1.373	11,220(E)	0.57	4.29(-17)		?
1-Methoxy-4-nitrobenzene	305	1			153.14	1.2192	10,600(M)	0.47	4.05(-17)		1.507
Nitrosobenzene	304	1			107.11	z5	7224(E)	0.45	2.76(-17)		?
4-Dinitrobenzene	[l]301	1			168.11	1.625	[l]2150(M)	0.11	8.22(-18)		?
4-Nitrosophenol	298	2			123.11	z6	15,300(M)	1.01	5.85(-17)		?
2,4-Dinitrophenol	[a]292	2	d, h		184.11	1.683	[a]10,000(A)	0.49	3.82(-17)		?
2-Nitrobenzaldehyde	[l]290	2			151.12	1.2844	[l]1300(Hx)	0.059	4.97(-18)		?
3-Nitrobenzaldehdye	[l]289	2			151.12	1.2792	[l]1000(Hx)	0.045	3.83(-18)		?
Nitrobenzene	[k]280	2			123.11	1.2037	[k]7974	0.40	3.04(-17)		1.5562
4-Nitrobenzaldehyde	[l]265	2			151.12	1.496	[l]10,800(M)	0.52	4.13(-17)		?
2-Methyl-4,6-dinitrophenol (dinitrocres.)	263	2	h		198.14	?	?(M)	?	?		?
6-Methyl-2,4-dinitrophenol	?	?	i		198.14	?	?	?	?		?
2-Methyl-6-nitrophenol	?	1	d		153.14	?	?	?	?		?
3-Methyl-2-nitrophenol	?	?	i		153.14	?	?	?	?		?
3-Methyl-4-nitrophenol	?	?	d		153.14	?	?	?	?		?
4-Methyl-2-nitrophenol	?	?	i		153.14	1.2399	?	?	?		1.5744
4-Methyl-3-nitrophenol	?	?			153.14	?	?	?	?		?
Benzaldehydes											
2,5-Dimethoxybenzaldehdye	355	2			166.18	z7	5129(Cx)	0.21	1.96(-17)		?
2-Hydroxy-3-methoxybenzaldehyde	340	2			152.15	z7	2820(M)	0.12	1.08(-17)		?
2-Hydroxy-4,6-dimethoxybenzaldehyde	330	1			182.18	z7	3802(E)	0.13	1.45(-17)		?
2-Hydroxybenzaldehyde	[l]326	2		o	122.12	1.1674	[l]3600(E)	0.21	1.38(-17)		1.574
3,5-Dimethoxybenzaldehdye	325	2			166.18	z7	2512(Cx)	0.10	9.60(-18)		?
2-Methoxybenzaldehyde	[l]322	1			136.15	1.1326	[l]4600(E)	0.23	1.76(-17)		1.56
3-Hydroxybenzaldehyde	[a]316	2			122.12	1.1179	[a]3162(A)	0.17	1.21(-17)		?
4-Hydroxybenzaldehyde	315	2			122.12	1.129	2640(M)	0.14	1.01(-17)		1.5705
2,4-Dimethoxybenzaldehyde	314	1			166.18	z7	9490(M)	0.34	3.63(-17)		?
3-Methoxybenzaldehdye	310	1		n,o	136.15	1.1187	2570(M)	0.12	9.83(-18)		1.553
4-Hydroxy-3,5-dimethoxybenzaldehyde	309	2			182.18	z7	14,454(E)	0.47	5.52(-17)		?
3-Methoxy-4-hydroxybenzaldehyde	309	2			152.15	1.056	10,471(E)	0.41	4.00(-17)		?
3,4-Dimethoxybenzaldehdye	307	2		n,o	166.18	z7	9170(M)	0.33	3.51(-17)		?
2,5-Dimethylbenzaldehyde	303	?		n	134.18	0.95	1810(M)	0.07	6.92(-18)		?

Table 3. (continued)

Chemical Name	λ_p nm	S	Ref. A	Ref. B	m g mol^{-1}	ρ g cm^{-3}	ε M^{-1} cm^{-1} (Solvent)	κ	b_{liq} cm^2 molecule^{-1}	b_{gas} cm^2 molecule^{-1}	n
Benzaldehyde	290	2			106.12	1.0415	1000(Hx)	0.05	3.82(-18)	[s]2.80(-17)	1.5463
1,3-Benzenedicarboxaldehyde	289	2			134.13	z7	1050(M)	0.043	4.01(-18)		?
3-Methylbenzaldehyde	288	2		n,o	120.15	1.0189	1514(I)	0.07	5.79(-18)		1.5413
2-Methylbenzaldehyde	280	2		n,o	120.15	1.0328	872(M)	0.039	3.33(-18)		1.5462
2,4,6-Trimethylbenzaldehyde	264	1		n	148.20	1.0154	10,600(M)	0.35	4.05(-17)		?
2,4-Dimethylbenzaldehdye	258	?		n	134.18	z7	13,400(M)	0.49	5.12(-17)		?
4-Methylbenzaldehyde	255	2		n,o	120.15	1.0194	21,300(M)	0.85	8.14(-17)		1.5454
Other aldehydes											
Acrolein	[l]351	4			56.06	0.84	[l]20(Hx)	0.0019	7.65(-20)		1.4017
Crotonaldehyde	[l]341	3			70.09	0.8516	[l]24(Hx)	0.0018	9.18(-20)		1.4366
Formaldehyde	330	3	c		30.03	0.815	4(C5)	0.0007	1.52(-20)	[t]3.32(-20)	?
Methacrolein	[a]330	5			70.09	0.84	[a]13(Hp)	0.001	4.97(-20)		1.4144
Benzeneacetaldehyde	300	2			120.15	1.0272	100(E)	0.005	3.82(-19)		1.5255
Acetaldehyde	292	5			44.05	0.7834	10(Hp)	0.0010	3.82(-20)	[t]4.68(-20)	1.3316
Butyraldehyde	283	3			72.11	0.8016	13(W)	0.0008	4.97(-20)	[g]4.80(-20)	1.3843
Benzoic acids											
2-Hydroxybenzoic acid	300	2			138.12	1.443	794(W)	0.046	3.04(-18)		1.565
3,5-Dimethylbenzoic acid	291	2			150.18	z8	1210(M)	0.06	4.62(-18)		?
3,4-Dimethoxybenzoic acid	290	1		o	182.18	z8	5470(M)	0.23	2.09(-17)		?
4-Methylbenzoic acid	280	1		n,o	136.15	z9	614(M)	0.025	2.35(-18)		?
Benzoic acid	279	2		n,o	122.12	1.2659	729(M)	0.039	2.79(-18)		1.504
2-Methylbenzoic acid	278	1			136.15	1.062	1250(M)	0.05	4.78(-18)		1.512
Aromatic polycarboxylic acids											
Trimellitic acid	296	4	m		210.14	z10	1585(W)	0.09	6.06(-18)		?
Pyromellitic acid	291	2	m		254.15	z10	2040(M)	0.1	7.80(-18)		?
Terephtalic acid	286	1	m		166.13	z10	1960(D)	0.14	7.49(-18)		?
Phtalic acid	[a]281	2	m		166.13	2.18	[a]1259(A)	0.09	4.81(-18)		?
Isophtalic acid	[a]280	2	m		166.13	z10	[a]1259(A)	0.09	4.81(-18)		?
Other acids											
Pyruvic acid	[a]330	5	r		88.06	1.2272	[a]20(A)	0.0017	7.65(-20)		1.4280
Propionic acid	270	5			74.08	0.993	?(W)	?	?		1.3809
Nicotinic acid	262	2		p	123.11	1.473	2750(M)	0.16	1.05(-17)		?
Phenols											
1,4-Benzenediol	294	3	g	p	110.11	1.328	2810(M)	0.19	1.07(-17)		?
2-Methyl-1,4-benzenediol	292	4			124.14	?	?(M)	?	?		?
4-Methylphenol (*p*-Cresol)	[l]286	2	e,i		108.14	1.0185	[l]2050(Hp)	0.10	7.84(-18)	[s]2.00(-18)	1.5312
4-Methyl-1,2-benzenediol	283	3		p	124.14	1.1287	?(M)	?	?		1.5425
4-Propyl-1,3-benzenediol	281	3			152.19	z11	2800(M)	0.11	1.07(-17)		?
1,2-Benzenediol	278	4	g	p	110.11	1.1493	?(M)	?	?		1.604
3-Methylphenol (*m*-Cresol)	278	2	i		108.14	1.0341	?(M)	?	?	[s]1.00(-17)	1.5438
3-Methyl-1,2-benzenediol	275	3			124.14	z11	21,200(M)	0.97	8.11(-17)		?
Phenol	[l]275	3	c,e,i		94.11	1.0545	[l]1200(W)	0.068	4.59(-18)	[s]2.50(-17)	1.5408
1,3-Benzenediol	275	3	g		110.11	1.2717	?(M)	?	?		?
2-Methylphenol (*o*-Cresol)	273	3	e,i		108.14	1.135	1820(M)	0.096	6.96(-18)	[s]1.65(-17)	1.5361
Alkanals and alkanones											
Decanal	293	1		j	156.27	0.83	25(Dc)	0.0007	9.56(-20)		1.4287
2-Undecanone	279	1		j	170.3	0.825	?(Cx)	?	?		1.4291
Aromatic hydrocarbons											
Anthracene	376	1	e,g	n,p	178.23	1.28	7590(M)	0.14	1.72(-17)		?
Benzo[b]fluoranthene	369	1	m,q	n,o	252.32	z12	6918(E)	0.24	2.65(-17)		?
Fluoranthene	357	1	e,g,q	n,o,p	202.26	1.252	8400(M)	0.34	3.21(-17)		?
Acenaphthylene	339	1	e,g		152.2	0.8987	4510(M)	0.17	1.72(-17)		?
Pyrene	334	?	e,g,m,q	n,o,p	202.26	1.271	29,400(M)	1.13	1.12(-16)		?
Benzo[a]pyrene	[l]333	?	e	e	252.32	z12	[l]39,000(Hp)	0.94	1.49(-16)		?
Benzo[e]pyrene	332	?	m	n,o	252.32	z12	31,623(E)	0.98	1.21(-16)		?
Acenaphthene	320	1	e,g		154.21	1.0242	1430(M)	0.06	5.46(-18)		1.6048
Chrysene	319	1	e,g,m,q	n,o,p	228.29	1.274	12,200(M)	0.40	4.66(-17)		?

Table 3. (continued)

Chemical Name	λ_p nm	*S*	Ref. A	Ref. B	*m* g mol^{-1}	ρ g cm^{-3}	ε M^{-1} cm^{-1} (Solvent)	κ	b_{liq} cm^2 molecule^{-1}	b_{gas} cm^2 molecule^{-1}	*n*
2-Methylnaphthalene	318	1	b,e,g		142.20	1.0058	515(M)	0.021	1.97(-18)		1.6015
Naphthalene	311	1	b,c,e,g		128.17	1.0253	239(M)	0.011	8.14(-19)		1.5898
Fluorene	300	1	e,g		166.22	1.203	10,000(E)	0.40	3.82(-17)		?
Phenanthrene	291	1	e,g	n,o,p	178.23	0.98	12,800(M)	0.38	4.89(-17)		1.5943
1,3,5 Trimethylbenzene	282	1			120.19	0.8652	17,400(M)	0.65	6.65(-17)		1.4994
Organic bases											
1-Methyl isoquinoline	320	2	m		143.19	1.0777	2818(Hx)	0.13	1.08(-17)		1.6095
Isoquinoline	[l]318	1	g,m	n	129.16	1.091	[l]3650(Hp)	0.18	1.40(-17)		1.6148
2,4-Dimethylquinoline	315	2	g		157.22	1.0611	?(M)	?	?		1.6075
Quinoline	[l]308	1	g	n	129.16	1.0977	[l]3850(M)	0.18	1.47(-17)		1.6268
Indole	[l]287	3	g		117.15	1.22	[l]4250(Hp)	0.23	1.62(-17)		?
Miscellaneous											
Carbazole	[l]337	1	b,g		167.21	z13	[l]3150(E)	0.19	1.20(-17)		?
Retene	300	1	m		234.34	1.035	14,800(M)	0.36	5.66(-17)		?

Solubilities in water (*S*) are given on a relative scale: 1, insoluble; 2, slightly soluble; 3, soluble; 4, very soluble; 5, miscible. Ref. A references are those in which the aerosol phase of the substance was observed in ambient air or the laboratory. Ref. B. references are those in which the aerosol phase of the substance was observed in aerosol emissions. Data for UV absorption peak wavelengths, solubilities, molecular weights (*m*), species densities (ρ), liquid-phase molar absorption coefficients, base 10 (ε), and real refractive indices (*n*) were obtained from *Lide and Milne* [1995], except where specified at the end of this footnote. Data for imaginary refractive indices (κ) were calculated from equation (4). Liquid-phase molecular absorption cross sections, base *e* (b_{liq}) were calculated from equation (6). Gas-phase molecular absorption cross sections, base *e* (b_{gas}) were obtained from the literature. A (?) indicates the data were not available. 1.0(-17) reads 1.0 x 10^{-17}.

Density substitutes: use values from 2,4-dinitrophenol (z1), 2-nitrophenol (z2), 1,3-benzenediol (z3), isoquinoline (z4), nitrobenzene (z5), 4-nitrophenol (z6), benzaldehyde (z7), 2-hydroxybenzoic acid (z8), 2-methylbenzoic acid (z9), phtalic acid (z10), 4-methyl-1,2-benzenediol (z11), anthracene (z12), estimated as 1.6 (z13). Solvents used to determine absorption coefficients: A, alcohol (either methyl or ethyl); C, 0.1M HCl; Cx, cyclohexane; C5, i-C_5H_{12}; D, dioxane; Dc, decane; E, ethyl alcohol; Hp, heptane; Hx, hexane; I, isooctane; M, methyl alcohol; N, Na salt/water solution; W, water.

[a]*Hirayama* [1969].
[b]*Schuetzle et al.* [1975].
[c]*Cronn et al.* [1977].
[d]*Nojima et al.* 1983].
[e]*Pankow et al.* [1983].
[f]*Grosjean* [1985].
[g]*Finlayson-Pitts and Pitts* [1986].
[h]*Rippen et al.* [1987].
[i]*Leuenberger et al.* [1988].
[j]*Rogge et al.* [1991].
[k]*Foster* [1992].
[l]*Perkampus* [1992].
[m]*Rogge et al.* [1993a].
[n]*Rogge et al.* [1993b].
[o]*Rogge et al.* [1993c].
[p]*Rogge et al.* [1994].
[q]*Venkataraman et al.* [1994].
[r]*Saxena and Hildemann* [1996].
[s]*Trost et al.* [1997].
[t]*Atkinson et al.* [1997].

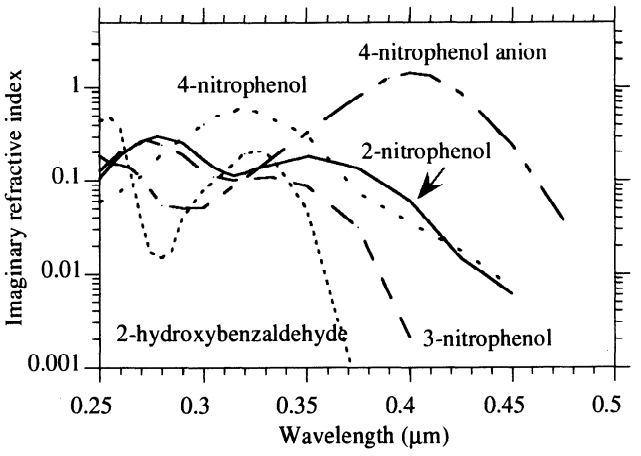

Figure 2. Imaginary indices of refraction of five nitrated and/or aromatic particulate organic substances observed in the atmosphere or in emissions (see Table 3 for observation references). Values were calculated from (6) using information (densities, molecular weights) from Table 3 and spectral molar absorption coefficient data (ε, base 10) from *Perkampus* [1992].

derived from (4) and from data of *Perkampus* [1992], of the anionic versus molecular form of 4-nitrophenol as a function of wavelength.

Table 3 shows similar characteristics for several dimethylnitrophenols dissolved in sodium salt/water (basic) solutions. The pH of these solvents may have caused the seven dimethylnitrophenols to ionize, since all had peak absorption wavelengths ≥0.4 μm. The three dimethylnitrophenols dissolved in other solvents were probably in their molecular forms, since their peak absorption wavelengths were less than 0.36 μm. 3,6-Dimethyl-2-nitrophenol had a peak absorption wavelength of 0.424 μm when dissolved in the sodium solution, but a peak of 0.347 μm when dissolved in ethanol. Absorption enhancement at high pH may be an important at Riverside, where high particulate ammonium concentrations are likely to increase the aerosol pH.

4.4. Absorption by Inorganic Nitrates

Although atmospheric models have not considered UV absorption by ammonium nitrate, this crystal also absorbs UV radiation shorter than 0.357 μm, with its longest wavelength peak occurring at 0.308 μm [*Cleaver et al.*, 1963]. Similarly,

sodium nitrate absorbs at a peak near 0.298 μm [*Cleaver et al.*, 1963], and the nitrate ion absorbs at a peak of 0.3025 μm [*Sommer*, 1989]. The magnitude of ammonium nitrate absorption is not strong, but not negligible, especially at photolytically important wavelengths. From Figure 4 of *Cleaver et al.* [1963], which gives percent absorption of incident radiation through an ammonium nitrate lattice as a function of wavelength, and from a minimum lattice thickness of 3 μm (p. 442), (3) gives the upper limit of ammonium nitrate's imaginary refractive index $\kappa = 0.0083$ at 0.308 μm. This upper limit decreases with wavelength to zero at 0.357 μm. The nitrate concentration during SCAQS reached 25 μg m^{-3} at Claremont and 64 μg m^{-3} at Riverside on August 27, 1987 at 1230 PST. The combination of its high concentrations and moderate / low imaginary index may make inorganic nitrate a nontrivial UV absorber in Los Angeles air at certain wavelengths, although it is probably less important than many other absorbers.

4.5. Absorption by Gas-Phase Nitrated Aromatics, Phenols, and Aldehydes

Many of the nitrated aromatics, phenols, and aldehydes in Table 3 appear in the gas as well as aerosol phase. Gas-phase molecular absorption cross-section data compiled by *Atkinson et al.* [1997] indicate that the common gas-phase aldehydes and ketones, such as formaldehyde, acetaldehyde, benzaldehyde, methacrolein, and methylvinylketone are relatively weak absorbers at UV wavelengths >295 nm. Nevertheless, their absorption causes important phototransformations due to their relatively high quantum yields.

Trost et al. [1997] performed experiments and estimated absorption cross sections at wavelengths <295 nm for several gas-phase aromatics, including phenol, benzaldehyde, *p*-cresol, *m*-cresol, and *o*-cresol. Their results indicated that these aromatics are strong gas-phase absorbers below 295 nm. Gas-phase absorption cross sections for nitrated aromatics have not been tabulated. Here, it is hypothesized that the gas-phase absorption cross sections of nitrophenols and nitrocresol can be approximated as their respective liquid-phase peak absorption cross sections, given in Table 3 or, since the addition of a nitrate group to a benzene ring shifts the peak wavelength of absorption toward longer wavelengths, as the cross sections of gas-phase phenols and a cresol, shifted toward longer wavelengths. For this study the former approximation method is used.

Although nitrated and aromatic aerosols and nitrated aromatic gases strongly absorb in the UV spectrum, such reactions may not lead to significant photochemical reaction products. *Alif et al.* [1987, 1990, 1991] and *Alif and Boule* [1991] found that quantum yields for aqueous-phase nitrophenols ranged from 10^{-6} to 10^{-5} at long UV wavelengths, indicating inefficient phototransformation.

Because most nitrated and aromatic aerosols and nitrated aromatic gases are stronger absorbers of UV than visible radiation, they are likely to reduce UV much more than visible irradiance. This might explain why observed reductions in downward UV irradiance in Los Angeles were much larger than observed reductions in downward total solar irradiance. This hypothesis is tested below.

5. Column and Three-Dimensional Simulations

Column and three-dimensional (3-D) simulations were run to test the effects of nitrated and aromatic aerosols and nitrated aromatic gases on UV irradiance in the Los Angeles basin. The simulations were performed for August 27-28, 1987, with GATORM, a gas, aerosol, transport, radiation, and meteorological model [*Jacobson*, 1994, 1997a-c, 1998a-c; *Jacobson et al.*, 1996]. The meteorological component of the model was developed by *Lu and Turco* [1995]. GATORM is the first 3-D model in which gas, size-resolved aerosol, radiative, and meteorological predictions have been compared simultaneously with data from a comprehensive database [*Jacobson*, 1994; 1997b].

Jacobson [1997b] compared 3-D predictions from the model with data for many gas, aerosol, radiative, and meteorological parameters without consideration for the effects of UV absorption by nitrated and aromatic species. Figures 14-18 and Table 3 of that paper compared predicted with observed near-surface particulate organic carbon (OC) concentrations. Table 3 indicated that daytime near-surface OC concentrations were generally underpredicted in the model, but Figures 14-18 of that paper indicated that some daytime peaks were captured. Also shown were comparisons of predicted with observed near-surface total particulate mass, elemental carbon, sodium, ammonium, sulfate, nitrate, chloride, visible scattering extinction, and visible absorption extinction. These figures indicated how predicted near-surface particulate loadings, similar to those used for the present 3-D simulations, compared with observations.

Jacobson [1998c] compared predictions from the same 3-D model with ozone and temperature data to estimate the effects of the UV reductions on photolysis coefficients, ozone, and temperatures. In that paper and here, the model grid southwest corner was located at 32.97°N latitude and 119.25°W longitude. The horizontal spherical coordinate grid included 66 west-east by 42 south-north grid cells. Grid spacing was 0.05° west-east (about 4.6 km) and 0.045° south-north (about 5.0 km). In the vertical, 20 sigma-pressure coordinate layers between the topographical surface and 250 mbar were used. Approximately eight layers resided below 850-mbar (1.5 km) altitude. In the previous work the model treated 111 gases (242 kinetic reactions and 29 photolysis reactions) and 36 aerosol components in each of the 16 size bins. In this work, 111 gases, 37 aerosol components and 17 aerosol size bins were used.

Most remaining parameters and processes solved for in the present simulations were the same as those of *Jacobson* [1998c], except as described next. First, absorption by nitrated aromatic gases was accounted for here but not in the previous work. Second, three types of size-distributed organic aerosol components were assumed here: directly emitted organics, liquid nitrocresol formed from gas-to-particle conversion, and all other organics formed from gas-to-particle conversion. In the previous work, only directly emitted organics and total organics formed from gas-to-particle conversion were considered in optical calculations.

Nitrocresol was assigned as an explicit aerosol species here, since its predicted gas-phase concentrations in eastern Los Angeles together with its saturation vapor pressure indicated that it was the most likely gas-phase nitrated aromatic included

in the gas-phase chemical mechanism to condense onto aerosols. The longest peak absorption wavelength and the corresponding imaginary refractive index of liquid nitrocresol are given in Table 3. The peak was scaled for other wavelengths with the absorbance distribution for 2,4-dinitrophenol, given in Figure 2 of *Lipczynska-Kochany* [1992]. Remaining condensed/dissolved organics were assumed to have the peak absorption wavelength and imaginary refractive index of terephtalic acid (Table 3). The peak was scaled for other wavelengths with the imaginary refractive index distribution for nitrobenzene, shown in Figure 1. Terephtalic acid was chosen simply because it has been observed in ambient particles and its longest peak wavelength (0.286 μm) falls between those of many nonnitrated organics in Table 3 and those of many monocarboxylic and dicarboxylic acids with shorter peak wavelengths, not appearing in Table 3. Directly emitted organics were assumed to have the peak absorption wavelength and imaginary refractive index of 3,4-dimethoxybenzaldehyde (Table 3). The peak was also scaled for other wavelengths with the imaginary refractive index distribution for nitrobenzene. This substance was chosen, since it has been observed in particle emissions and had an average peak wavelength in comparison with all benzaldehydes in Table 3.

The model accounted for wavelength-dependent refractive indices of 37 solid and liquid aerosol components, including those of the three organic components. A Mie algorithm for stratified spheres, originally by *Toon and Ackerman* [1981], was used to estimate absorption, forward, and total scattering efficiencies. For visible wavelengths and when particles contained less than 0.1% liquid nitrocresol, elemental carbon was assumed to be core material, and the mixture of all other components was assumed to be shell material. When particles contained more than 0.1% liquid nitrocresol, nitrocresol was assumed to be shell material for UV wavelengths, and the mixture of all other components was assumed to be core material. Remaining aspects of radiative calculations are described by *Jacobson* [1998c].

The nitrated aromatic gases considered in the model included nitrocresol (a generalized methylnitrophenol), a generalized nitrophenol, and peroxybenzoyl nitrate. The photochemical reactions for these species were obtained from the expanded carbon bond IV mechanism [*Gery et al.*, 1989]. Nitrocresol and nitrophenol are end-products in the reaction mechanism. At each time step, condensational growth equations for nitrocresol were solved between the gas phase and all 17 aerosol size bins with the Analytical Predictor for Condensation (APC) scheme [*Jacobson*, 1997c]. The saturation vapor pressure used for nitrocresol was 8.0×10^{-6} Pa [*Pilinis and Seinfeld*, 1988].

Condensation/dissolution of other organics was accounted for by assuming that a fraction of certain organic gases, such as benzaldehyde, peroxybenzoyl nitrate, cresol, and nitrophenol, among others, could convert to condensable products. The fractions were obtained from aerosol yields of *Pandis et al.* [1992]. Those yields gave the mass concentration of aerosol formed per unit emissions of an organic precursor. Instead of applying the yields to emissions, the yields were applied to gases as they formed chemically, which allowed certain emitted organics to react in the gas phase before their products were converted to the particle phase. At each time step, a fraction of each aerosol-producing gas was combined into one generalized condensable gas. Condensational growth equations were then solved between the lumped gas and the 17 aerosol size bins (where the aerosol component was "all other non-primary organics") with the APC scheme. The saturation vapor pressure was assumed to be that of adipic acid, given by *Pilinis and Seinfeld* [1988].

Gas-phase extinction coefficients were calculated for 41 gases, including 29 organic gases. Some of the organics included nitrocresol, nitrophenol, phenol, formaldehyde, acetaldehyde, benzaldehyde, cresol, peroxybenzoyl nitrate, methacrolein, acetone, methylvinylketone, methyl hydroperoxide, peroxyacetylnitrate, methylperoxy nitric acid, ethylperoxy nitric acid, propylperoxy nitric acid, methyl nitrite, methyl nitrate, ethyl nitrate, and propyl nitrate.

5.1. Column Simulations

Several column radiative transfer simulations within the 3-D grid domain were run for 1230 PST on August 27. During these static (time-independent) runs, irradiance reductions were calculated at Claremont and Riverside. Initial near-surface gas, aerosol, and meteorological fields were interpolated or extrapolated from observations at 1230 over the three-dimensional domain from SCAQS data. Aerosol data used for interpolations included near-surface concentrations of sulfate, nitrate, chloride, sodium, ammonium, organic carbon, and elemental carbon in sub-2.5- and sub-10-μm particles. Calcium and magnesium concentrations were estimated from measurements taken on August 28.

Measured particulate OC concentrations were divided into primary OC, nitrocresol, and other OC. Aerosol nitrocresol (surrogate for nitrated aromatic aerosol) concentrations were set to 12% of total OC at downtown Los Angeles, where the observed nitrate to OC ratio was about 1:1 (Table 2), but scaled to other locations with the observed nitrate:OC ratio. Since the nitrate:OC ratio increases from about 1.0 at Los Angeles to 4 at Riverside, it is expected that the concentration of nitrated aromatics (whether primary or secondary) at Riverside exceeded that at Los Angeles. *O'Brien et al.* [1975] and *Mylonas et al.* [1991] estimated that organic nitrates made up 12-21% of total organic mass in Los Angeles. Other nonprimary OC concentrations in the model were set to 15% of total OC. The remaining OC was assigned to primary OC. *Pandis et al.* [1992] estimated that about 73-85% of total OC mass at inland locations in Los Angeles was primary OC mass.

Aerosol mass concentrations near Claremont and Riverside were assumed to increase in concentration from the ground to middle boundary layer, then decrease toward the top of the boundary layer, in order to account for elevated aerosol layers. Middle-tropospheric aerosol masses were assumed to be the same as those from *Li et al.* [1997]. Concentrations from the boundary layer top were interpolated with pressure between the boundary layer and middle troposphere.

Aerosol mass components at each altitude and location were distributed over quadramodal lognormal distributions, as described by *Jacobson* [1997a, p. 141]. The chemical equilibrium solver, EQUISOLV II (*Jacobson*, 1998d) was then used to estimate aerosol composition and liquid water content (due to hydration) in each size bin. The code considered equilibrium and mixed activity coefficient equations among sodium, chloride, potassium, calcium, magnesium, sulfate,

nitrate, chloride, and carbonate substances in the ionic, liquid, and / or solid phases. Temperatures and relative humidities, used in the code, were obtained from sounding data. Once composition was calculated, the solution density in each bin was obtained by combining ions into electrolytes and using the method described by *Tang* [1997]. The solution density was combined with solid densities to estimate volumes and radii of particles in each bin. The resulting profiles of predicted aerosol PM 2.5 and PM 10 (aerosols in particles less than 2.5 and 10 μm in diameter, respectively) at Claremont and Riverside are given in Figure 3. The figure also shows near-surface observations of these parameters.

Baseline column radiative calculations were then performed to estimate the attenuation of downward global UV and total solar irradiances at 1230 on August 27. Figure 3 shows the resulting irradiance profiles. The predicted values at the surface

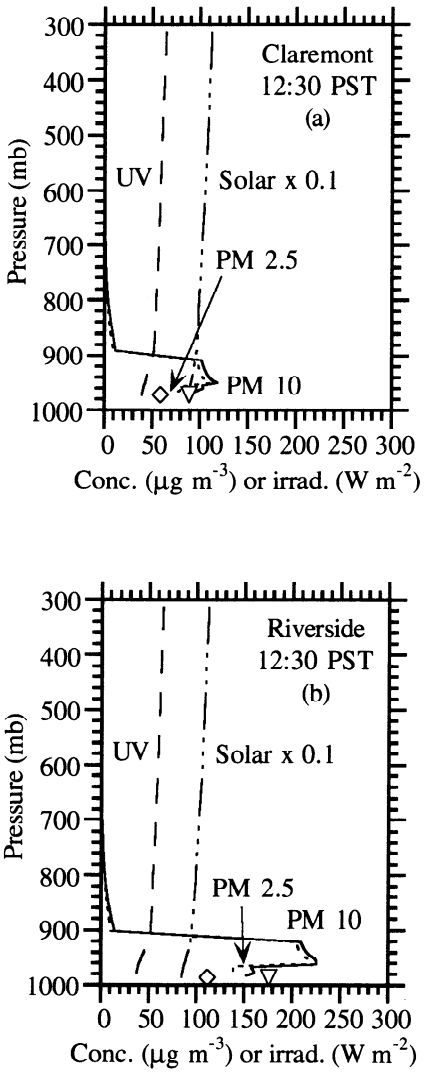

Figure 3. Predicted sub-2.5 and sub-10 μm-diameter (PM 2.5 and PM 10, respectively) aerosol mass concentrations, downward global UV (0.295-0.385 μm) irradiance, and downward global solar irradiance (0.285-2.8 μm) at (a) Claremont and (b) Riverside on August 27, 1987, at 1230 PST, from the baseline column simulation. The diamond and triangle are observed near-surface PM 2.5 and PM 10 concentrations, respectively. Observed near-surface UV and solar irradiance data are given in Table 4 for comparison.

are also compared with observations in Table 4 (baseline versus observed cases). Figure 4 shows predicted extinction coefficients due to gas and aerosol scattering and absorption at three wavelengths from the column simulations. Measurements of visible-light aerosol scattering and absorption extinction coefficients are shown in Figures 4c and 4f for comparison. Comparisons of predicted versus observed near-surface visible extinction coefficients from column experiments at Claremont, Riverside, and other sites are given in Table 5.

At 0.305 μm, ozone dominated gas extinction (with coefficients between 0.05 and 0.07 km^{-1}). At 0.32 μm, NO_2 dominated gas extinction (coefficients between 0.01 and 0.05 km^{-1}). Because gas-phase nitrocresol concentrations were limited by the nitrocresol saturation vapor pressure in the baseline simulation, its extinction coefficient was limited to about 0.005 - 0.007 km^{-1} at 0.305 and 0.32 μm. Gas scattering was the dominant UV extinction process above the boundary layer. Aerosol scattering dominated aerosol absorption in UV and visible wavelengths, although the ratio of absorption:scattering extinction increased from the visible to the UV. *Jacobson* [1998c] predicted the ratio to exceed unity at Claremont on August 27 at 1130 PST during a 3-D simulation; but the optical properties of nitrated and aromatic aerosols were updated here in comparison with that work.

Table 4 shows statistics for UV and total solar irradiance from observations, the baseline case, and several sensitivity tests. The table shows that the baseline-predicted UV surface irradiance predictions were 1.5 and 6.8 W m^{-2} larger than observations at Claremont and Riverside, respectively. Since the observed reductions were 18.6 and 27.2 W m^{-2}, respectively (Table 4), the model underpredicted the UV irradiance reductions by 8.1 and 25% at the respective locations, even when nitrated and aromatic aerosol and nitrated aromatic gas absorption were accounted for.

Several sensitivity tests were run to examine the extent to which different assumptions affected predicted UV reductions. Table 4 shows that ignoring UV absorption by organic aerosols (test 1) lessened downward UV irradiance reductions by 4.4 and 6.4 W m^{-2} at Claremont and Riverside, respectively. Thus organic aerosol absorption appears to have accounted for about 23.7% (100% x 4.4 / 18.6) and 23.5% (100% x 6.4 / 27.2) of the total observed downward UV attenuation at these respective locations. Tests 2 and 3 break down these statistics further. Test 2 indicates that nonnitrated aromatics accounted for 13.5 and 8.8% of the downward reductions at Claremont and Riverside, respectively, and test 3 indicates that nitrated aromatics accounted for 10.2 and 14.7% of the reductions.

Test 4 indicates that ignoring absorption by inorganic aerosol nitrate components lessened UV reductions by 0.02 and 0.1 W m^{-2} at Claremont and Riverside, respectively. Thus inorganic aerosol nitrate absorption may have accounted for only 0.1 and 0.4% of the total observed downward UV attenuation at these locations. The relative ratio at the two sites is due to the fact that inorganic nitrate concentrations were higher at Riverside than at Claremont.

Test 5 indicates that removing all gas absorption lessened UV irradiance reductions by 2.4 and 1.6 W m^{-2} at Claremont and Riverside, respectively. Thus total gas absorption may have accounted for about 12.9 and 5.9% of the total observed downward UV attenuation at these locations. Total gas absorption extinction at Claremont exceeded that at Riverside

Table 4. Downward Global UV and Total Solar Surface Irradiances From Observations, Predicted From the Baseline Case, and Predicted From Several Sensitivity Cases at 1230 PST on August 27 at Claremont and Riverside

	Claremont		Riverside	
	UV W m^{-2}	Total Solar W m^{-2}	UV W m^{-2}	Total Solar W m^{-2}
"Observed" at 1.7 km*	56.5	986	56.5	986
Observed at surface	37.9	--	29.3	852
Observed attenuation between 1.7 km and surface	18.6	--	27.2	134
Baseline prediction at surface (LNC shell, mixed core in UV, mixed shell, EC core in visible)	39.4	881	36.1	848
Sensitivity tests				
1. No UV POC, NNOC, or LNC absorption	43.8 (+4.4)	885 (+4)	42.5 (+6.4)	855 (+7)
2. No UV POC or NNOC absorption	41.9 (+2.5)	883 (+2)	38.5 (+2.4)	850 (+2)
3. No UV LNC absorption	41.3 (+1.9)	883 (+2)	40.1 (+4.0)	853 (+5)
4. No inorganic nitrate absorption	39.4 (+0.02)	881 (+0)	36.2 (+0.1)	848 (+0)
5. No gas absorption	41.8 (+2.4)	888 (+7)	37.7 (+1.6)	855 (+7)
6. No nitrated aromatic gas absorption	40.6 (+1.2)	882 (+1)	37.2 (+0.9)	849 (+1)
7. Set GNC=50 times its saturation vapor pressure	35.9 (-3.5)	877 (-4)	31.8 (-4.3)	843 (-5)
8. Double κ for LNC	38.8 (-0.6)	880 (-1)	34.5 (-1.6.)	846 (-2)
9. Triple κ for LNC	38.5 (-0.9)	880 (-1)	33.8 (-2.3)	845 (-3)
10. Reduce κ for LNC by half	39.8 (+0.4)	881 (0)	37.3 (+1.2)	849 (+1)
11. Shift LNC absorption +30 nm	39.1 (-0.3)	880 (-1)	35.4 (-0.7)	847 (-1)
12. Shift LNC absorption -30 nm	39.7 (+0.3)	881 (0)	36.9 (+0.8)	849 (+1)
13. Double κ, shift absorption +30 nm for LNC	38.5 (-0.9)	879 (-2)	33.7 (-2.4)	844 (-4)
14. Set κ of POC and NNOC to that of LNC	37.9 (-1.5)	875 (-6)	35.4 (-0.7)	845 (-3)
15. Mixed shell, EC core in UV and visible	41.4 (+2.0)	882 (+1)	39.2 (+3.1)	850 (+2)
16. AN shell, mixed core in UV, mixed shell, EC core in visible	39.2 (-0.2)	880 (-1)	35.5 (-0.6)	847 (-1)
17. Multiply elevated aerosol concentrations by 1.5	36.2 (-3.2)	857 (-14)	31.7 (-4.4)	815 (-33)
18. Raise top height of elevated layer by 20 mb	38.3 (-1.1)	872 (-9)	33.6 (-2.5)	829 (-19)

The numbers in parentheses are the differences (W m^{-2}) between the sensitivity test prediction and the baseline prediction. Predictions were obtained from the column simulations. LNC, liquid nitrocresol; GNC, gas-phase nitrocresol; EC, elemental carbon; POC, primary organic carbon; NNOC, nonnitrated secondary organic carbon = total organic - POC - LNC; and AN, ammonium nitrate.

*"Observed" UV values at 1.7 km were estimated as those at Mount Wilson on August 27, 1987, and "observed" visible values at 1.7 km were estimated as those at Mount Disappointment on September 2, 1973.

at 1230 PST, simply because NO_2 concentrations were higher at Claremont than at Riverside at this time. Removing only nitrated aromatic gas absorption (test 6) lessened UV irradiance reductions by 1.2 and 0.9 W m^{-2}. Thus nitrated aromatic gas absorption may have accounted for about 6.5 and 3.3% of the total observed downward UV attenuation, or about half the attenuation caused by all gas absorption at Claremont and Riverside, respectively. Nitrated aromatic gases attenuated total solar radiation much less than did other absorbing gases, since some other gases, particularly NO_2, absorbed in the visible spectrum as well as in the UV.

Summing statistics from tests 1, 4, and 6 gives total UV reduction estimates due to nitrated and aromatic aerosols and nitrated aromatic gases as 5.6 and 7.4 W m^{-2}, or 30% and 27% of the observed downward irradiance reductions at Claremont and Riverside, respectively.

When the initial boundary layer concentration of gas-phase nitrocresol was assumed to be 50 times its saturation vapor pressure (equivalent to twice the observed toluene plus xylene concentrations at 1230 PST at both locations) (test 7), 3.5 and 4.3 W m^{-2} in additional downward irradiance reductions were calculated at Claremont and Riverside, respectively. This assumption improved the predicted UV irradiance at Riverside in comparison with the observation. Since the corresponding changes in total solar irradiance were no greater than the changes in the UV irradiance, the assumption of additional nitrated aromatic gas absorption is convenient for explaining the difference between the baseline prediction and observations. However, the high nitrated aromatic gas concentrations, required for this explanation, have yet to be measured.

The next seven sensitivity tests involved changing the magnitude or shifting the peak wavelength of the imaginary indices of refraction of organic components. Doubling κ at all UV wavelengths for liquid nitrocresol (test 8) increased downward UV reductions at Claremont and Riverside by 0.6 and 1.6 W m^{-2}, respectively. Tripling κ (test 9) increased UV reductions at Claremont and Riverside by 0.9 and 2.3 W m^{-2}, respectively. In both cases, total solar reductions changed about the same as total UV reductions. Reducing κ by one-half (test 10) reduced UV reductions by 0.4 and 1.2 W m^{-2}, at Claremont and Riverside, respectively. Shifting liquid nitrocresol absorption by 30 nm toward longer wavelengths (test 11) increased reductions by 0.3 and 0.7 W m^{-2}, respectively. Shifting absorption by 30 nm toward shorter wavelengths (test 12) decreased reductions by 0.3 and 0.8 W m^{-2}, respectively. Doubling κ together with shifting liquid nitrocresol absorption by 30 nm toward longer wavelengths

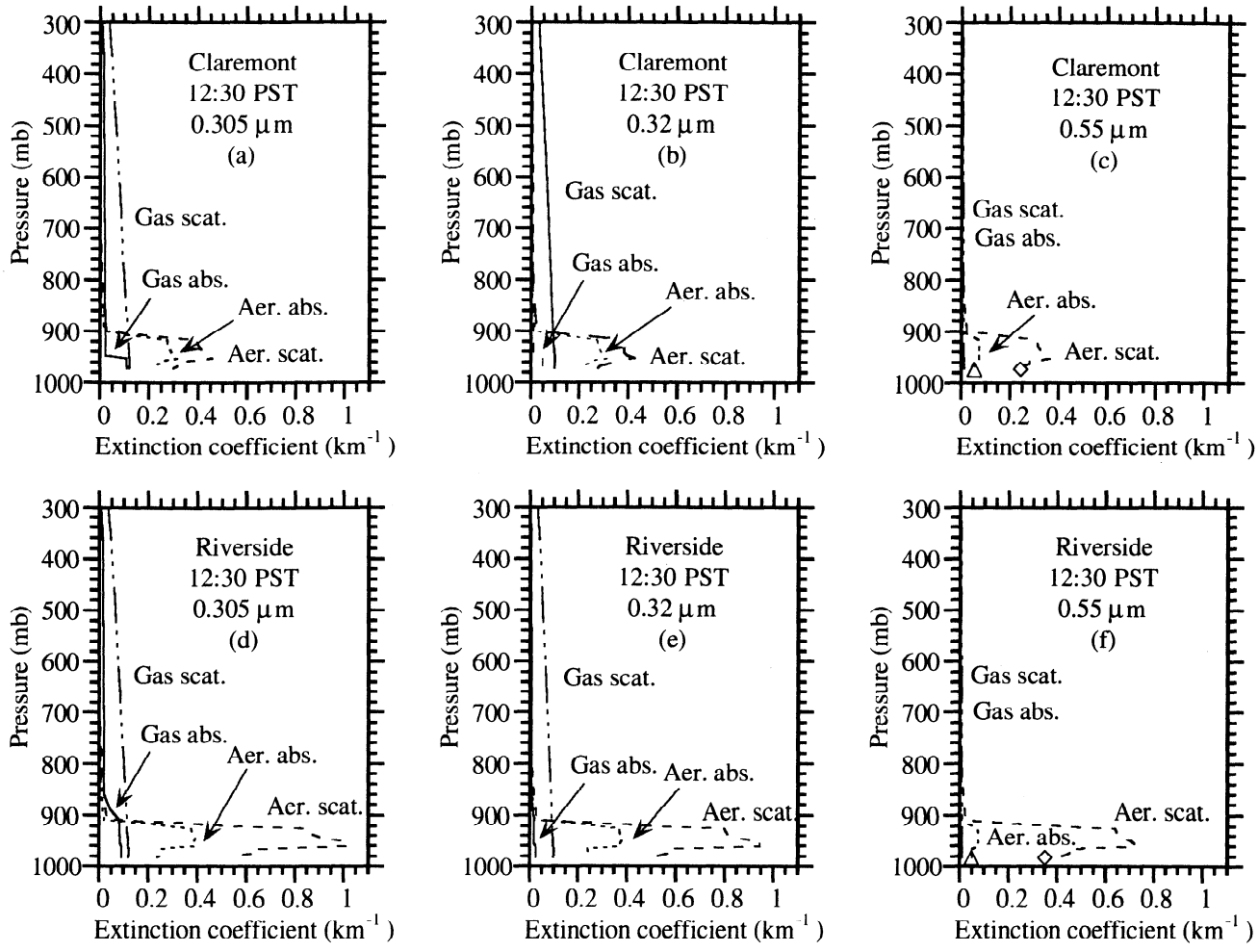

Figure 4. Predicted vertical profiles, from Claremont and Riverside at 1230 PST, August 27, 1987, of extinction coefficients (km^{-1}) due to gas scattering, aerosol scattering, gas absorption, and aerosol absorption at bands centered at (a, d) 0.305, (b, e) 0.32 μm, and (c, f) 0.55 μm for the baseline column simulation. The triangle and diamond in Figures 4c and 4f are measurements. Absorption coefficient measurements were at 0.55 μm. The Claremont and Riverside scattering coefficient measurements were at 0.475 μm and 0.525 μm, respectively.

Table 5. Comparison of Predicted with Observed Near-Surface Absorption and Scattering Extinction Coefficients at All Sites in Which the Measurements Were Available at 1230 PST on August 27, 1987

	Predicted σ_a km^{-1}	Observed σ_a km^{-1}	Difference %	Predicted σ_s km^{-1}	Observed σ_s km^{-1}	Difference %
Anaheim	0.047	0.044	6.8		--	
Azusa	0.075	0.071	5.6		--	
Burbank	0.081	0.072	12.5		--	
Los Angeles	0.059	0.050	18.0		--	
Claremont	0.054	0.053	1.8	0.23	0.24	-4.2
Hawthorne	0.009	0.012	-25.8		--	
Long Beach	0.027	0.024	12.5	0.17	0.25	-32
Riverside	0.049	0.048	2.1	0.40	0.35	14.3

Predictions were obtained during the column simulations. Aerosol loadings were initialized at 1230 PST from observations. Absorption coefficient measurements were made at 0.55 μm. The Claremont scattering coefficient measurements were made at 0.475 μm. Those at Long Beach and Riverside were made at 0.525 μm.

(test 13) increased reductions by 0.9 and 2.4 W m^{-2}, respectively. This scenario could occur if nitrated aromatics were anionic and had the absorption characteristics similar to those of 4-nitrophenol. Finally, setting κ's for all organic aerosol components to those of liquid nitrocresol (test 14) increased reductions by 1.5 and 0.7 W m^{-2}, respectively. In sum, while uncertainties in the imaginary indices of refraction of organics used undoubtedly affect the results, they do not appear to have accounted for most of the differences between the baseline predictions and the observations.

Test 15 involved calculating UV extinction coefficients with the same technique as visible extinction coefficients, namely assuming an elemental carbon core and a shell made up of all other components, with a refractive index, averaged by mass over all such components. In the baseline case the shell was assumed to be nitrocresol so long as particles contained >0.1% nitrocresol, and the core had a refractive index averaged by mass over all core components. Test 15 resulted in lesser UV irradiance reductions of 2.0 and 3.1 W m^{-2} at Claremont and Riverside, respectively, than in the baseline simulation. Thus the baseline assumption appeared to simulate the data better. When ammonium nitrate, instead of liquid nitrocresol, was

assumed to be shell material for UV wavelengths (thus nitrocresol was mixed in with other core material) (test 16), UV reductions were increased by 0.2 and 0.6 W m^{-2} at Claremont and Riverside, respectively. Thus this assumption slightly improved prediction accuracy. Assuming ammonium nitrate is shell material may be more realistic than assuming nitrocresol is shell material, since ammonium nitrate concentrations were much larger than those of nitrocresol. Both are formed by gas-to-particle conversion.

Tests 17 and 18 involved changing concentrations and height, respectively, of the elevated aerosol layer. Multiplying aerosol concentrations in the elevated layer by 1.5 increased UV reductions by 3.2 and 4.4 W m^{-2} at Claremont and Riverside, respectively. Raising the top height of the elevated layer by 20 mbar increased the reductions by 1.1 and 2.5 W m^{-2}. In both cases the additional total solar reductions were excessively large because enhancement of the elevated layers increased concentrations of UV- and visible-scattering aerosol components as well as UV-reducing components. The resulting predicted total solar irradiance were much lower than observations. These tests lend further credence to the theory that preferential UV absorption, whether by gases or aerosols, may have caused even more UV reductions than predicted in the baseline case.

5.2. Three-Dimensional Simulations

Three-dimensional simulations were run from 0330 PST, August 27 to 2330 PST, August 28, 1987. Gas and aerosol fields (including aerosol size distributions) were initialized over the 3-D grid in the same manner as with the column simulations, except that observations at 0330 PST on August 27 were used in this case. Initial aerosol fields were affected, over time, by emissions, nucleation, coagulation, condensation, dissolution, reversible chemistry, irreversible chemistry, dry deposition, sedimentation, and transport. Initial gas fields were affected by emissions, gas chemistry, condensation, dissolution, dry deposition, and transport. After initialization, observations were used only for comparison with model predictions. Thus size-distributed concentrations of organic and other aerosol components were predicted at all locations in the model domain.

Three simulations were run. In the first, aerosols were excluded from the model, and nitrated aromatic gas absorption was ignored (gas-only simulation). In the second, aerosols were included in the calculations, but absorption by nitrated and aromatic aerosols and nitrated aromatic gases was ignored. In this case, predictions of UV irradiance reductions were similar to those shown in Table 4, sensitivity test 1, and 3-D results are not shown. In the third simulation (final-aerosol simulation), aerosols were included, and absorption by nitrated and aromatic aerosols and nitrated aromatic gases absorption was accounted for. Conditions for this simulation were similar to those for the baseline simulation of Table 4.

Figure 5 shows predictions of downward global surface solar irradiances (0.285-2.8 μm) at Mount Wilson and Riverside (CM44) from the gas-only and final-aerosol simulations for August 27-28, 1987. Figure 5a compares predictions with observations from Mount Disappointment, obtained from *Peterson et al.* [1978] for September 2, 1973. The observations at Mount Disappointment are shown, since no elevated measurements of downward total solar irradiance at Mount Wilson were made during SCAQS. Mount Disappointment (elevation 1820 m) is only a few kilometers west of Mount Wilson (1739 m), and observations of downward solar irradiance at these elevations are unlikely to vary significantly from year-to-year for a given day of the year. Figure 5b compares predictions with observations at Riverside from SCAQS. The figures indicate that gases and aerosols in the boundary layer reduced peak observed downward total solar irradiance between the elevations of Mount Disappointment and Riverside by about 14%. Differences between the gas-only and final-aerosol simulations indicate that gas scattering and absorption caused a 3% reduction in total solar irradiance, while aerosol scattering and absorption caused an 11% reduction.

Figure 6 compares gas-only and final-aerosol simulation predictions with observations of downward global UV (0.295-0.385 μm) surface irradiances at Mount Wilson, Los Angeles, Claremont, and Riverside. Downward UV irradiances were overpredicted the most at Riverside, just as they were in the column simulations. The UV reductions due to all gas and aerosol components between Mount Wilson and the surface, predicted in the 3-D simulations, were about 30% at Claremont

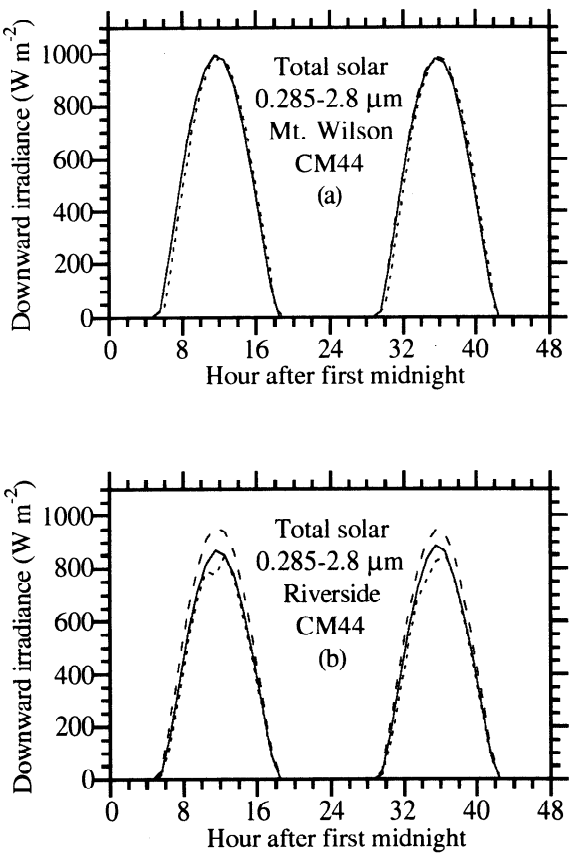

Figure 5. Comparison of downward global surface solar irradiance (0.285-2.8 μm) predicted when aerosols were accounted for (solid lines, final aerosol simulation), predicted when aerosols were excluded (long-dashed lines, gas-only simulation), and observed (short-dashed lines) at (a) Mount Wilson and (b) Riverside on August 27 - 28, 1987. The observations at Mount Wilson are really observations (obtained from *Peterson et al.* [1978]) from September 2, 1973, at Mount Disappointment repeated for both days at Mount Wilson. Mount Disappointment is a few kilometers to the west of and 80 m taller than Mount Wilson. Predictions were obtained from 3-D simulations.

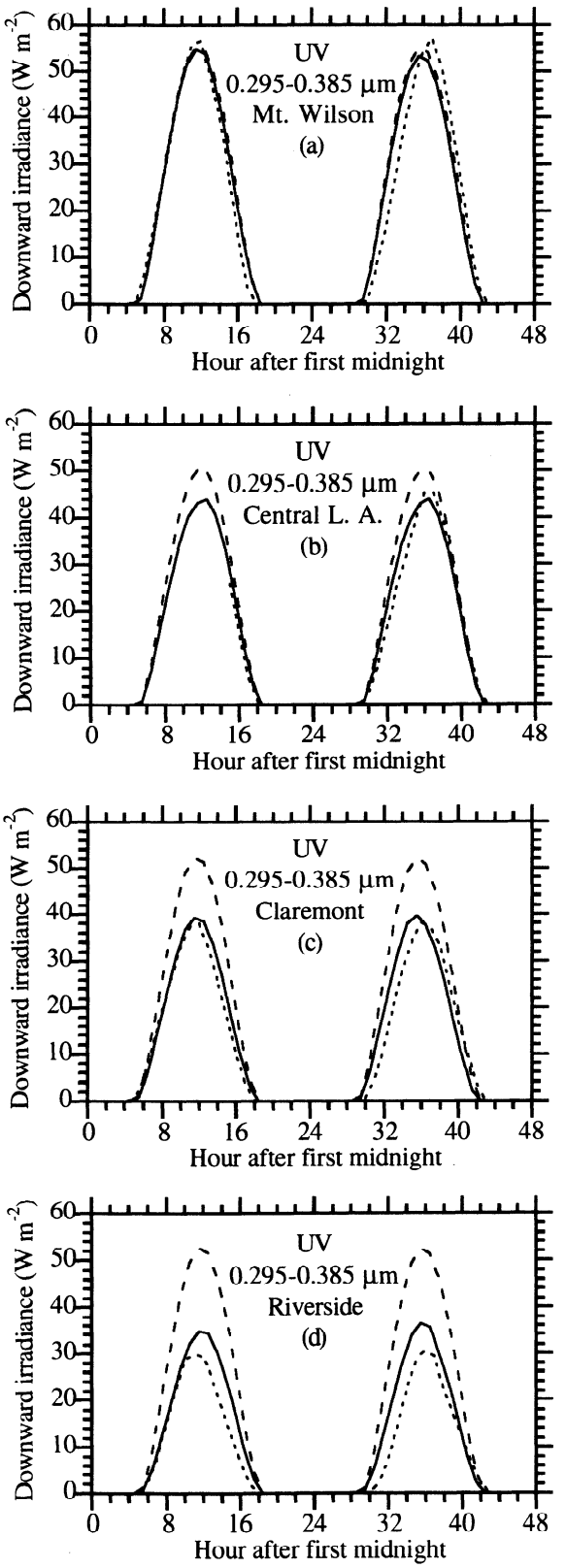

Figure 6. Comparison of downward global surface UV irradiances (0.295-0.385 μm) predicted when aerosols were accounted for (solid lines, final aerosol simulation), predicted when aerosols were excluded (long-dashed lines, gas-only simulation), and observed (short-dashed lines) on August 27 - 28, 1987, at four locations. Observed data for central Los Angeles were available beginning at 1500 on August 27. Predictions were obtained from 3-D simulations.

and 36% at Riverside. The predicted reductions between Mount Wilson and central Los Angeles were about 20%. The predicted reductions were less than the observed reductions of 33%, 48%, and 22%, respectively, at these three sites. Nevertheless, they were about 30% greater, than the reductions resulting when absorption by nitrated and aromatic aerosols and nitrated aromatic gases was ignored in the model.

A consequence of the predicted decrease in UV irradiance due to aerosol absorption was a decrease in ozone mixing ratios of 5-8% [*Jacobson*, 1998c]. Despite these reductions, ozone mixing ratios were still the highest in the United States in August, 1987. Ozone reductions were also accompanied by the presence of high particle loadings.

While this study hypothesizes that UV absorption by organic and nitrated inorganic components within aerosols occurs and may be important in urban regions (and to a lesser extent in free tropospheric regions), further laboratory, field experiments, and modeling studies (including closure studies) are needed to better quantify the extent of such absorption. The data needed include wavelength-dependent real and imaginary refractive indices of individual aerosol components, vertical profiles of measured size-distributed organic aerosol constituents, and vertical profiles of measured UV irradiance and aerosol scattering and absorption extinction coefficients.

6. Summary

Absorption by nitrated and aromatic aerosols and nitrated aromatic gases were hypothesized to have reduced observed downward global UV irradiance between Mount Wilson and sites within the boundary layer in the Los Angeles basin during August 1997. Likely organic UV absorbers are nitrated aromatics, benzaldehydes, other aldehydes, benzoic acids, aromatic polycarboxylic acids, phenols, polycyclic aromatic hydrocarbons, and certain organic bases. Ammonium nitrate, sodium nitrate, and the nitrate ion also have moderate to small absorption capabilities below 0.4 μm. Because absorption by nitrated and aromatic compounds tail off between the UV and visible spectra, predicted reductions of downward global UV irradiance were enhanced much more than were those of total solar irradiance. Reductions in UV irradiance were found to reduce ozone mixing ratios in Los Angeles by 5-8%. Ozone mixing ratios were still the highest in the United States during this period. Since organic carbon and nitrate have been widely observed in particles beyond urban regions, they may affect UV extinction coefficients in such regions. Further laboratory and field studies are needed to quantify better the extent of UV absorption by organic components within aerosols.

Acknowledgments. This work was supported, in part, by grants from the Environmental Protection Agency under assistance agreement 823186-01-0, the National Science Foundation under agreements ATM-9504481 and ATM-9614118, and the David and Lucile Packard Foundation and the Hewlett-Packard company through a Stanford University Terman Fellowship.

References

Alif, A., and P. Boule, Photochemistry and environment, XIV, Phototransformation of nitrophenols induced by excitation of nitrite and nitrate ions, *J. Photochem. Photobiol. A Chem.*, *59*, 357-367, 1991.

Alif, A., P. Boule, and J. Lemaire, Comportement photochimique du nitro-4 phonol en solution aqueuse, *Chemosphere*, *16*, 2213-2223, 1987.

Alif., A., P. Boule, and J. Lemaire, Photochemistry and environment, XII, Phototransformation of 3-nitrophenol in aqueous solution, *J. Photochem. Photobiol. A Chem.*, *50*, 331-342, 1990.

Alif, A., J.-F. Pilichowski, and P. Boule, Photochemistry and environment, XIII, Phototransformation of 2-nitrophenol in aqueous solution, *J. Photochem. Photobiol. A Chem*, *59*, 209-219, 1991.

Ambach, W., and M. Blumthaler, Characteristics of solar UV irradiance, *Meteorol. Z.*, *3*, 211-220, 1994.

Atkinson R., D. L. Baulch, R. A. Cox, R. F. Hampson Jr., J. A. Kerr, M. J. Rossi, and J. Troe, Evaluated kinetic, photochemical, and heterogeneous data for atmospheric chemistry, Supplement V, *J. Phys. Chem. Ref. Data*, *26*, 521-1011, 1997.

Beyer, K. D., A. R. Ravishankara, and E. R. Lovejoy, Measurements of UV refractive indices and densities of H_2SO_4/H_2O and $H_2SO_4/HNO_3/H_2O$ solutions, *J. Geophys. Res.*, *101*, 14,519 - 14,524, 1996.

Blumthaler, M., W. Ambach, and W. Rehwald, Solar UV-A and UV-B radiation fluxes at two Alpine stations at different altitudes, *Theor. Appl. Meteorol.*, *46*, 39-44, 1992.

Blumthaler, M., A. R. Webb, G. Seckmeyer, A. F. Bais, M. Huber, and B. Mayer, Simultaneous spectroradiometry: A study of solar UV irradiance at two altitudes, *Geophys. Res. Lett.*, *21*, 2805-2808, 1994.

Chow, J. C., J. G. Watson, E. M. Fujita, Z. Lu, and D. R. Lawson, Temporal and spatial variations of $PM_{2.5}$ and PM_{10} aerosol in the Southern California Air Quality Study, *Atmos. Environ.*, *28*, 2061-2080, 1994.

Cleaver, B., E. Rhodes, and A. R. Ubbelohde, Studies of phase transformations in nitrates and nitrites, I, Changes in ultra-violet absorption spectra on melting, *Proc. R. Soc. London*, *276*, 437-453, 1963.

Cronn, D. R., R. J. Charlson, R. L. Knights, A. L. Crittenden, and B. R. Appel, A survey of the molecular nature of primary and secondary components of particles in urban air by high-resolution mass spectrometry, *Atmos. Environ.*, *11*, 929-937, 1977.

Dean, J. A., *Lange's Handbook of Chemistry*, McGraw-Hill, New York, 1992.

Dickerson, R. R., S. Kondragunta, G. Stenchikov, K. L. Civerolo, B. G. Doddridge, and B. N. Holben, The impact of aerosols on solar UV radiation and photochemical smog, *Science*, *278*, 827-830, 1997.

Finlayson-Pitts, B. J., and J. N. Pitts Jr., *Atmospheric Chemistry: Fundamentals and Experimental Techniques*, John Wiley, New York, 1986.

Forster, P. M. de F., Modeling ultraviolet radiation at the earth's surface, I, The sensitivity of ultraviolet irradiances to atmospheric changes, *J. Appl. Meteorol.*, *34*, 2412-2425, 1995.

Foster, V. G., Determination of the refractive index dispersion of liquid nitrobenzene in the visible and ultraviolet, *J. Phys. D. Appl. Phys.*, *25*, 525-529, 1992.

Gery, M. W., G. Z. Whitten, J. P. Killus, and M. C. Dodge, A photochemical kinetics mechanism for urban and regional scale computer modeling, *J. Geophys. Res.*, *94*, 12,925-12,956, 1989.

Gillette, D. A., E. M. Patterson Jr., J. M. Prospero, and M. L. Jackson, Soil aerosols, in *Aerosol Effects on Climate*, edited by S. G. Jennings, Univ. of Ariz. Press, Tucson, 1993.

Grosjean, D., Reactions of o-cresol and nitrocresol with NO_x in sunlight and with ozone-nitrogen dioxide mixtures in the dark, *Environ. Sci. Technol.*, *19*, 968-974 1985.

Hirayama, K., *Handbook of Ultraviolet and Visible Absorption Spectra of Organic Compounds*, Plenum, New York, 1967.

Jackson, J. D., *Classical Electrodynamics*, John Wiley, New York, 1975.

Jacobson, M. Z., Developing, coupling, and applying a gas, aerosol, transport, and radiation model to study urban and regional air pollution, Ph.D. thesis, Univ. of Calif., Los Angeles, 1994.

Jacobson, M. Z., Development and application of a new air pollution modeling system, part II, Aersosol module structure and design, *Atmos. Environ.*, *31*, 131-144, 1997a.

Jacobson, M. Z., Development and application of a new air pollution modeling system, part III, Aerosol-phase simulations, *Atmos. Environ.*, *31*, 587-608, 1997b.

Jacobson, M. Z., Numerical techniques to solve condensational and dissolutional growth equations when growth is coupled to reversible reactions, *Aerosol Sci. Technol.*, *27*, 491-498, 1997c.

Jacobson, M. Z., Improvement of SMVGEAR II on vector and scalar machines through absolute error tolerance control, *Atmos. Environ.*, *32*, 791-796, 1998a.

Jacobson, M. Z., *Fundamentals of Atmospheric Modeling*, Cambridge Univ. Press, New York, 1998b.

Jacobson, M. Z., Studying the effects of aerosols on vertical photolysis rate coefficient and temperature profiles over an urban airshed, *J. Geophys. Res.*, *103*, 10,593-10,604, 1998c.

Jacobson, M. Z., Studying the effects of calcium and magnesium on size-distributed nitrate and ammonium with EQUISOLV II, *Atmos. Environ.*, in press, 1998d.

Jacobson, M. Z., R. Lu, R. P. Turco, and O. B. Toon, Development and application of a new air pollution modeling system, part I, Gas-phase simulations, *Atmos. Environ.*, *30B*, 1939-1963, 1996.

Kato, S., T. P. Ackerman, E. E. Clothiaux, J. H. Mather, G. G. Mace, M. L. Wesely, F. Murcray, and J. Michalsky, Uncertainties in modeled and measured clear-sky surface shortwave irradiances, *J. Geophys. Res.*, *102*, 25,881-25,898, 1997.

Krekov, G. M. Models of atmospheric aerosols, in *Aerosol Effects on Climate*, edited by S. G. Jennings, Univ. of Ariz. Press, Tucson, 1993.

Leuenberger, C., J. Czuczwa, J. Tremp, and W. Giger, Nitrated phenols in rain: Atmospheric occurrence of phytotoxic pollutants, *Chemosphere*, *17*, 511-515, 1988.

Li, S.-M.K, A. M. Macdonald, J. W. Strapp, Y.-N. Lee, and X.-L. Zhou, Chemical and physical characterizations of atmospheric aerosols over southern California, *J. Geophys. Res.*, *102*, 21,341-21,353, 1997.

Lide, D. R., and G. W. A. Milne (Eds.), *Handbook of Data on Common Organic Compounds*, CRC Press, Boca Raton, Fla., 1995.

Lipczynska-Kochany, E., Degradation of nitrobenzene and nitrophenols in homogeneous aqueous solution. Direct photolysis versus photolysis in the presence of hydrogen peroxide and the Fenton reagent, *Water Pollut. Res. J. Can.*, *27*, 97-122, 1992.

Liousse, C., J. E. Penner, C. Chuang, J. J. Walton, H. Eddleman, and H. Cachier, A global three-dimensional model study of carbonaceous acrosols, *J. Geophys. Res.*, *101*, 19,411-19,432, 1996.

Liu, S. C., S. A. McKeen, and S. Madronich, Effect of anthropogenic aerosols on biologically active ultraviolet radiation, *Geophys. Res. Lett.*, *18*, 2265 - 2268, 1991.

Lu, R., and R. P. Turco, Air pollutant transport in a coastal environment, II, Three-dimensional simulations over Los Angeles basin, *Atmos. Environ.*, *29*, 1499 - 1518, 1995.

Lu, Y., and M. A. K. Khalil, The distribution of solar radiation in the earth's atmosphere: The effects of ozone, aerosols, and clouds, *Chemosphere*, 32, 739 - 758, 1996.

Madronich, S., Photodissociation in the atmosphere, 1, Actinic flux and the effects of ground reflections and clouds, *J. Geophys. Res.*, *92*, 9740-9752, 1987.

Mylonas, D. T., D. T. Allen, S. H. Ehrman, and S. E. Pratsinis, The source and size distributions of organonitrates in Los Angeles aerosol, *Atmos. Environ.*, *25A*, 2855-2861, 1991.

Nojima, K., A. Kawaguchi, T. Ohya, S. Kanno, and M. Hirobe, Studies on photochemical reactions of air pollutants, X, Identification of nitrophenols in suspended particulates, *Chem. Pharmacol. Bull*, *31*, 1047-1051, 1983.

Novakov, T., D. A. Hegg, and P. V. Hobbs, Airborne measurements of carbonaceous aersosols on the East Coast of the United States, *J. Geophys. Res.*, *102*, 30,023-30,030, 1997.

O'Brien, R. J., J. H. Crabtree, J. R. Holmes, M. C. Hoggan, and A. H. Bockian, Formation of photochemical aerosol from hydrocarbons, *Environ. Sci. Technol.*, *9*, 577-582, 1975.

Pandis, S. N., R. A. Harley, G. R. Cass, and J. H. Seinfeld, Secondary organic aerosol formation and transport, *Atmos. Environ.*, *26A*, 2269-2282, 1992.

Pankow, J. F., L. M. Isabelle, W. E. Asher, T. J. Kristensen, and M. E. Peterson, Organic compounds in Los Angeles and Portland rain: Identities, concentrations and operative scavenging mechanisms, In *Precipitation Scavenging, Dry Deposition and Resuspension*, edited by H. R. Pruppacher, R. G. Semonin, and W. G. N. Slinn, p. 403, Elsevier, New York, 1983.

Peterson, J. T., E. C. Flowers, and J. H. Rudisill, Urban-rural solar radiation and atmospheric turbidity measurements in the Los Angeles basin, *J. Appl. Meteorol.*, *17*, 1595-1609, 1978.

Perkampus, H.-H., *UV-VIS Atlas of Organic Compounds*, 2nd ed., Weinheim, New York, 1992.

Pilinis, C., and J. H. Seinfeld, Development and evaluation of an Eulerian photochemical gas-acrosol model, *Atmos. Environ.*, *22*, 1985-2001, 1988.

Reiter, R., K. Munzert, and R. Sladkovic, Results of 5-year concurrent recordings of global, diffuse, and UV-radiation at three levels (700, 1800, and 3000 m a.s.l.) in the northern Alps, *Arch. Meteorol. Geophys. Bioklimatol., Ser. B.*, *30*, 1-28, 1982.

Repapis, C. C., H. T. Mantis, A. G. Paliatsos, C. M. Philandras, A. F.

Bais, and C. Meleti, Case study of UV-B modification during episodes of urban air pollution, *Atmos. Environ.*, *32*, 2203 - 2208, 1998.

Rippen, G., E. Zietz, R. Frank, T. Knacker, and W. Klopffer, Do airborne nitrophenols contribute to forrest decline?, *Environ. Technol. Lett.*, *8*, 475-482, 1987.

Rogge, W. F., L. M. Hildemann, M. A. Mazurek, G. R. Cass, and B. R. T. Simoneit, Sources of fine organic aerosol, 1, Charbroilers and meat cooking operations, *Environ. Sci. Technol.*, *25*, 1112-1125, 1991.

Rogge, W. F., M. A. Mazurek, L. M. Hildemann, and G. R. Cass, Quantification of urban organic aerosols at a molecular level: Identification, abundance, and seasonal variation, *Atmos. Environ.*, *27A*, 1309-1330, 1993a.

Rogge, W. F., L. M. Hildemann, M. A. Mazurek, and G. R. Cass, Sources of fine organic aerosol, 2, Noncatalyst and catalyst-equipped automobiles and heavy-duty diesel trucks, *Environ. Sci. Technol.*, *27*, 636-651, 1993b.

Rogge, W. F., L. M. Hildemann, M. A. Mazurek, and G. R. Cass, Sources of fine organic aerosol, 3, Road dust, tire debris, and organometallic brake lining dust: Roads as sources and sinks, *Environ. Sci. Technol.*, *27*, 1892-1904, 1993c.

Rogge, W. F., L. M. Hildemann, M. A. Mazurek, G. R. Cass, and B. R. T. Simoneit, Sources of fine organic aerosol, 6, Cigarette smoke in the urban atmosphere, *Environ. Sci. Technol.*, *28*, 1375-1388, 1994.

Ruggaber, A. R., R. Dlugi, and T. Nakajima, Modelling radiation quantities and photolysis frequencies in the troposphere, *J. Atmos. Chem.*, *18*, 171-210, 1994.

Saxena, P., and L. M. Hildemann, Water-soluble organics in atmospheric particles: A critical review of the literature and application of thermodynamics to identify candidate compounds. *J. Atmos. Chem.*, *24*, 57-109, 1996.

Schuetzle, D., D. Cronn, A. L. Crittenden, and R. J. Charlson, Molecular composition of secondary aerosol and its possible origin, *Environ. Sci. Technol.*, *9*, 838-845, 1975.

Sokolik, I., A. Andronova, and C. Johnson, Complex refractive index of atmospheric dust aerosols, *Atmos. Environ.*, *27A*, 2495-2502, 1993.

Sommer, L., *Analytical Absorption Spectrophotometry in the Visible and Ultraviolet*, Elsevier, New York, 1989.

Tang, I., Thermodynamic and optical properties of mixed-salt aerosols of atmospheric importance, *J. Geophys. Res.*, *102*, 1883-1893, 1997.

Toon, O. B., and T. P. Ackerman, Algorithms for the calculation of scattering by stratified spheres, *Appl. Opt.*, *20*, 3657-3660, 1981.

Trost, B., J. Stutz, and U. Platt, UV-absorption cross sections of a series of moncyclic aromatic compounds, *Atmos. Environ.*, *31*, 3999-4008, 1997.

van Weele, M., and P. G. Duynkerke, Effects of clouds on the photodissociation of NO_2: Observation and modelling, *J. Atmos. Chem.*, *16*, 231 - 255, 1993.

Varotsos, C. A., G. J. Chronopouos, S. Katsikis, and N. K. Sakellariou, Further evidence of the role of air pollution on solar ultraviolet radiation reaching the ground, *Int. J. Remote Sens.*, *16*, 1883 - 1886, 1995.

Venkataraman, C. J. M. Lyons, and S. K. Friedlander, Size distributions of polycyclic aromatic hydrocarbons and elemental carbon, 1, Sampling, measurement methods, and source characterization, *Environ. Sci. Technol.*, *28*, 555-582, 1994.

Wakimoto, R. M., and J. L. McElroy, Lidar observation of elevated pollution layers over Los Angeles, *J. Clim. Appl. Meteorol.*, *25*, 1583-1599, 1986.

Wang, P., and J. Lenoble, Comparison between measurements and modeling of UV-B irradiance for clear sky: a case study, *Appl. Opt.*, *33*, 3964-3971, 1994.

Wendisch, M., S. Mertes, A. Ruggaber, and T. Nakajima, Vertical profiles of aerosol and radiation and the influence of a temperature inversion: Measurements and radiative transfer calculations, *J. Appl. Meteorol.*, *35*, 1703-1715, 1996.

Wenny, B. N., J. S. Schafer, J. J. DeLuisi, V. K. Saxena, W. F. Barnard, I. V. Petropavlovskikh, and A. J. Vergamini, A study of regional aerosol radiative properties and effects on ultraviolet-B radiation, *J. Geophys. Res.*, *103*, 17,083-17,097, 1998.

Zeng, J., R. McKenzie, K. Stamnes, M. Wineland, and J. Rosen, Measured UV spectra compared with discrete ordinate method simulations, *J. Geophys. Res.*, *99*, 23,019-23,030, 1994.

M. Z. Jacobson, Department of Civil and Environmental Engineering, Terman Engineering Center, Room M-13, Stanford University, Stanford, CA 94305-4020. (E-mail: jacobson@ce.stanford.edu)

(Received May 6, 1998; revised October 12, 1998;
accepted October 14, 1998.)